

Motion induced Magnetic susceptibility and field map estimation in fMRI

D. Yeo¹, J. Fessler², and B. Kim³

¹tbyeo@umich.edu, ²fessler@eecs.umich.edu, ³boklyek@umich.edu, Ann Arbor, MI, United States

Introduction Echo-planar imaging (EPI) typically used in functional MRI (fMRI) time series with high speed pulse sequences adversely affects data by magnetic field-inhomogeneities and cause geometrical distortion. A static field-inhomogeneity map may be measured to correct for such distortions, but it does not account for dynamic changes in magnetic field due to head motion during the time series acquisition. Applying rigid body transformations to an observed static field map may not be appropriate in the presence of significant out-of-plane head rotations since field-inhomogeneities change nonlinearly. In this study we retrospectively estimate the object's magnetic susceptibility (χ) map from an observed susceptibility induced static field map using regularized image restoration principles. Given a 3D χ -map estimate, the susceptibility induced dynamic field maps can be computed by applying rigid body motion followed by 3D susceptibility voxel convolution (SVC). SVC [1] is a deterministic, physics-based discrete convolution model for computing field maps from χ maps. We estimate the χ -map from a measured high resolution 3D static field map using 3D regularized image restoration techniques, i.e., solving the inverse problem of the noisy forward SVC model. The approach is demonstrated with realistically simulated noisy 3D field maps of a spherical air pocket in water.

Methods It was shown [2] that the z -component of the χ -induced field map, $B_p(\mathbf{r})$, for an object with K disjoint compartments of constant χ values is,

$$\mathbf{B}_p(\mathbf{r}) = \frac{\chi(\mathbf{r})}{3} \mathbf{B}_0 + \frac{\hat{\mathbf{z}}}{4\pi} \sum_{k=1}^K (\chi_k^+ - \chi_k^-) \int_{S_k} \frac{z-z'}{|\mathbf{r}-\mathbf{r}'|^3} \mathbf{B}_0 \cdot d\mathbf{S}' \quad (1)$$

where \mathbf{r}' is a surface point on surface S_k , $\hat{\mathbf{z}}$ is a unit vector parallel to \mathbf{B}_0 , χ_k^+ and χ_k^- denote the susceptibilities outside and inside the k^{th} compartment, respectively, S_k is the k^{th} surface, \mathbf{r}' is a surface point, $d\mathbf{S}'$ is perpendicular to the surface at \mathbf{r}' . In the presence of out-of-plane rotations, the orientation of the surfaces with \mathbf{B}_0 , i.e., $\mathbf{B}_0 \cdot d\mathbf{S}'$, changes, resulting in nonlinear field map changes. $B_0 \cdot d\mathbf{S}'$ changes with out-of-plane rotations, thus, resulting in nonlinear field map changes. SVC applies Eq. 1 directly to voxels of an object.

$$\mathbf{B}_p(\mathbf{r}) \approx \mathbf{B}_0 \left[\frac{\chi(\mathbf{r})}{3} + \frac{1}{4\pi} \sum_{k=1}^K (\chi_k^+ - \chi_k^-) \int_{y_k^- - l_y/2, x_k^- - l_x/2}^{y_k^+ + l_y/2, x_k^+ + l_x/2} \frac{(z_k + l_z/2 - z)}{|\mathbf{r}-\mathbf{r}'|^3} dx' dy' \right]$$

$$\mathbf{B}_p(l, m, n) = \mathbf{B}_0 \sum_{l', m', n' \in \text{FOV}} \chi(l', m', n') d(l-l', m-m', n-n')$$

Regularized Inverse SVC: We use a quadratic penalized weighted least squares (QPWLS) approach [3] to estimate χ by minimizing, $\Psi(\chi) = \frac{1}{2} \|\mathbf{g} - \mathbf{D}\chi\|_W^2 + \beta \|\mathbf{C}\chi\|^2$

where \mathbf{g} is the observed static field map, \mathbf{W} is a voxel-weighting matrix with higher weights where MR image intensity is higher, β is a regularization parameter that determines the amount of smoothing, \mathbf{D} is the forward SVC matrix, and \mathbf{C} is a first order finite-differencing matrix.

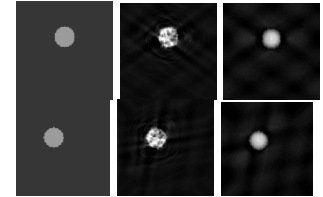
We simulated ground truth χ -maps of an off-centered spherical air ($\chi_{\text{air}}=0.04$ ppm) pocket in water ($\chi_{\text{water}}=-9.05$ ppm) that was rotated counterclockwise about the x -axis by angles from 0° (non-tilted position) to 180° , in increments of 2° . A SVC impulse response was formed and applied to the ground truth χ -maps with $B_0=1.5$ T to obtain ground truth field maps. In addition, a noisy static field map in the 0° position was simulated. The weighting matrix \mathbf{W} used is a simulated image intensity map, f , with zeros in the air pocket (no MR signal), and 100 in the water region.

Results The Wiener filter, and QPWLS method, were used to estimate static χ -maps (Fig 1) from the observed static field map. The same rotation angles used to generate the ground truths were applied to these χ -map estimates, and forward SVC was used to compute the dynamic field map estimates (Fig 2). The RMSE values over entire 3D field map estimates for all rotated positions using the various field map estimation methods are shown in Fig 3. It was observed that the QPWLS method had the best performing RMSE values, and RMSE variability, across all rotated positions.

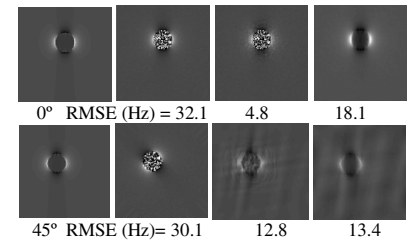
Conclusions Our work focuses on regularized image restoration methods to approximate dynamic field maps retrospectively without pulse sequence modifications. The proposed method estimates χ -induced dynamic field maps from an observed static χ -induced field map while accounting for the proper MR noise model. It does not require segmentation or pulse sequence modifications, and may yield higher resolution dynamic field maps that address nonlinear changes due to out-of-plane rotations. Unlike the Wiener filter, the proposed method does not require prior knowledge of object statistics. Further work will be to investigate methods to reliably measure non- χ induced field inhomogeneities, and characterize their effects. SVC is a deterministic, physics-based discrete convolution model for computing. An alternate way to approximate the object's χ -map would be to segment a T1-weighted anatomical reference volume into air, bone and soft tissue, and apply literature or approximated [Wells 2008] optimal susceptibility values to different voxels. Our approach obviates the burden of ensuring good accuracy in both the segmentation process, and the susceptibility values used.

References 1. Yoder, D.A., et al, Magn. Reson. Imag. 22, 315-328 (2004); 2. de Munck, J.C., et al IEEE Trans. Med. Imag. 15, 620-627 (1996); 3. Fessler, J.A.: Image reconstruction toolbox (2007).

Acknowledgments This research was supported in part by grant DHHS NIH P01 CA87634-01A2.



True χ Wiener filter QPWLS
Fig.1. χ -maps.



0° RMSE (Hz)= 32.1 4.8 18.1
45° RMSE (Hz)= 30.1 12.8 13.4
True B_p Observed B_p Wiener filter QPWLS
Fig 2. Field maps (-200 to 400 Hz). Top: non tilted field map slices. Bottom: 45° tilted positions.

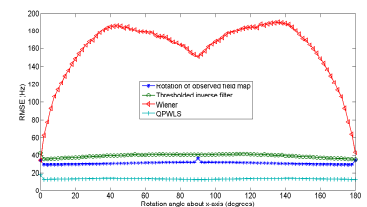


Fig. 3. Field map RMSE results for various rotation angles. Wiener filter uses flat object PSD.